Synsint Research Group

Available online at www.synsint.com

Synthesis and Sintering

**ISSN** 2564-0186 (Print), **ISSN** 2564-0194 (Online)

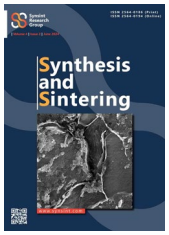


*Research article*

# On the synthesis and sintering behavior of a novel Mg-Ca alloy, Part II: Spark plasma sintering

**Parisa Golmohammadi** [a], **Ahmad Bahmani** [b], **Nader Parvin** [a,*], **Behzad Nayebi** [a,c,*]

[a] *Department of Materials and Metallurgical Engineering, Amirkabir University of Technology (Tehran Polytechnic), Tehran, Iran*
[b] *Department of Advanced Materials and Renewable Energy, Iranian Research Organization for Science and Technology, Tehran, Iran*
[c] *Arta Magnesium Parsian Engineering Co., Tehran, Iran*

ABSTRACT

With the growing interest in lightweight materials, magnesium and its alloys have received substantial attention for replacing existing alloys. After investigating the mechanical alloying process of Mg-Ca alloys and determining the optimum parameters for milling in part I of this study, the current research aims to examine the second step: the sintering process. This study proposes the powder metallurgy method to process Mg-Ca alloy through the spark plasma sintering technique at 420 °C under an applied pressure of 38 MPa. Samples with different additives (starch or paraffin) were sintered for various dwell times (7 and 10 min) to determine the optimal mechanical and physical properties. To study the microstructure and phase composition of the sintered alloys, X-ray diffractometer (XRD), field scanning electron microscopy (FESEM), and X-ray energy dispersive spectroscopy (EDS) were utilized. Density measurement, compression test, and micro-hardness evaluation were also conducted for the physical and mechanical feathers analysis. The results indicated that samples with a dwell time of 10 min exhibited superior mechanical properties. Additionally, the starch-containing sample outperformed the paraffin-containing sample in both physical and mechanical properties.


KEYWORDS

Spark plasma sintering
Magnesium
Powder metallurgy
Grain boundary
Strengthening
Solid solution strengthening

OPEN ACCESS

## 1. Introduction

Magnesium (Mg) has great potential in developing innovative materials, especially lightweight alloys due to its low density. Much effort has been devoted to studying its potential, including its dimensional stability, excellent biocompatibility, and biodegradability, leading to significant progress in recent decades [1–4]. Furthermore, magnesium is particularly attractive for various applications, from aerospace and lightweight structural components to biodegradable medical implants and automotive applications [5–8]. Nevertheless, despite Mg's significant benefits and applications in various industries, its weaknesses, such as low formability, poor mechanical strength, and high corrosion rate have constrained its large-scale applications [9–11]. As a result, the alloying process has emerged as a strategic approach to mitigate these limitations [12, 13]. However, it has now been accepted that some alloying elements, such as aluminum (Al), may exhibit toxicity or could potentially cause stress corrosion in the human body [14]. On the other hand, Calcium has a density close to magnesium and can enhance the corrosion resistance of the final alloy or assist in grain refinement [14].

Traditionally, magnesium-based materials were predominantly fabricated using conventional methods such as casting and deformation processing. However, due to magnesium's hexagonal crystal structure and a limited number of slip systems, deformation of its alloys at ambient temperatures is challenging. On the other hand, raising the temperature can lead to oxidation and adversely affect surface quality [15]. Hence, among the synthesis methods, powder metallurgy (PM) is a well-established and highly advantageous method, known for

* Corresponding authors. *E-mail address:* nparvin@aut.ac.ir (N. Parvin), behzad.nayebi@aut.ac.ir (B. Nayebi)
Received 20 December 2023; Received in revised form 20 June 2024; Accepted 23 June 2024.

https://doi.org/10.53063/synsint.2024.42194

achieving near-net-shape forming in complex shapes and refining grain structures. Moreover, it excels in overcoming typical limitations associated with conventional production techniques, resulting in improved mechanical properties of the final components through a uniform microstructure [16]. In this regard, the powder preparation stage, specifically the mechanical alloying (MA) process, can yield a fine microstructure with tailored mechanical characteristics [17].

In the previous work [18], the mechanical alloying technique was studied as the initial step of alloy formation. After investigating various parameters (milling time, additive type, and additive fraction), optimum milling parameters were identified that exhibited the best milling behavior and sinterability. The current and most important challenge facing with magnesium alloys is their high tendency to ignition due to the explosive nature of Mg. To overcome this issue, rapid sintering techniques are required.

As a result, the present study focuses on the sintering process of the powder alloy. Spark plasma sintering (SPS), characterized by its rapid heating rates, high applied pressures, and superior temperature uniformity, has recently been utilized to achieve rapid densification with minimal crystallization during consolidation [19–21]. This method has emerged as a solution to alleviate issues associated with prolonged sintering processes such as oxidation and the formation of undesirable secondary phases [22–24]. This advanced technique utilizes joule heating, where energy is supplied by passing an electric current through the particles. The powder mixtures are densely packed within the die and positioned between the electrodes [25–27]. When subjected to pressure and pulsed current, the temperature rises rapidly, and a spark discharge occurs either within gaps or at contact points between material particles. This phenomenon results in the evaporation and surface melting of powder particles, leading to the formation of "necks" between particles [28].

Within this paper, the sintering process of three distinct samples of Mg-Ca alloy is examined. The impacts of dwell time and additive type are the factors that have been investigated, providing valuable insights into the optimization of the alloy's properties.

## 2. Experimental

Initially, Mg-0.7 Ca alloy was prepared from magnesium (<45 µm, 99% purity), and Mg-7 wt% Ca master alloy (machined plates <100 µm, 99.9% purity). Fig. 1 illustrates the morphology and the elemental distribution of the starting as-milled powder mixtures. To mitigate oxidation of the Mg powder during milling and reduce powder adhesion to the milling media, paraffin or starch was added at a fraction of 2.5 wt%. Additionally, 1.5 wt% of stearic acid served as the process control agent (PCA) to minimize particle agglomeration. Mechanical alloying was carried out using a high-energy ball mill (SPEX 8000 M) for 60 min. Comprehensive details regarding the milling process can be found in the first part of this article [1].

After ball milling, the obtained powder mixtures were sintered in an SPS furnace (Nanozint, KPF Co., Iran), under the applied pressure of 38 MPa. The final temperature and the heating rate were 420 °C and 30 °C/min, respectively. The samples were SPSed with dwell times of 7 and 10 min to investigate the effects of dwell time on their characteristics. It should be highlighted that all the samples were kept at the temperature of 200–300 °C for 4 min during the heating up to evaporate the volatile compounds. The coding for the sintered samples is shown in Table 1.

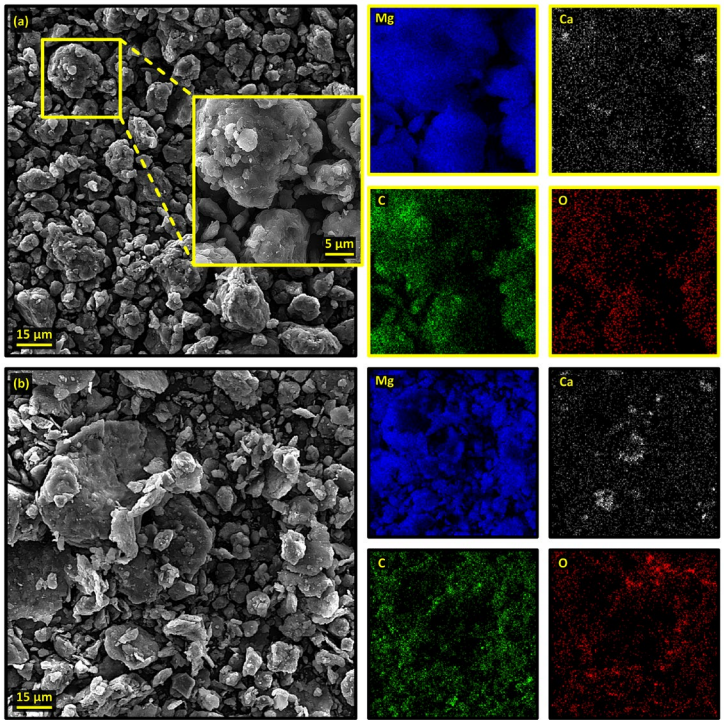


**Fig. 1.** The FESEM micrographs and related EDS elemental maps of the as-milled starting powder mixtures show the morphology and elemental distribution of a) starch-contained and b) paraffin-contained samples.

**Table 1.** Coding system of the sintered samples.

| Sample code | Dwell time (min) | Additive type |
|---|---|---|
| 7St | 7 | Starch |
| 10St | 10 | Starch |
| 10P | 10 | Paraffin |

**Table 2.** Relative density and water adsorption of the as-sintered samples.

| Sample code | Relative density (%) | Water adsorption (%) |
|---|---|---|
| 7St | ~100.00 | 0.11 |
| 10St | ~100.00 | 0.30 |
| 10P | ~100.00 | 0.16 |

The first step in characterizing the SPSed samples involved grinding them and measuring their densities using the Archimedes principle. To identify potential phases, the microstructure of the specimens was analyzed using X-ray diffraction spectroscopy (XRD, Philips PW1730) with Cu Kα radiation (λ = 1.5 Å). Field-emission scanning electron microscopy (FESEM, MIRA3, TESCAN) and energy dispersive spectroscopy (EDS: DXP-X10P) were employed to investigate the microstructure and elemental distribution of the as-SPSed samples. To evaluate the mechanical properties, the hardness was measured at room temperature using a Vickers microhardness tester (HV: Zwick Roell ZHV10) with a 100 g load for 15 s. The compression test was conducted at room temperature with an initial strain rate of $1.4\times10^{-3}$ $s^{-1}$ and a speed of 0.085 mm/min on rectangular samples (height: 6 mm, and area of base: 16 $mm^2$).

## 3. Results and discussion

The relative densities (RD) and water adsorption (WA) of the as-SPSed samples are presented in Table 2. The results indicate that all three samples are nearly fully dense. However, the water adsorption data suggests that sample 10St has a higher percentage of porosity. To draw a more comprehensive conclusion, this data should be integrated with displacement-time-temperature (DTT) diagrams, microstructural observations, and mechanical test results.

The DTT diagrams comprise four distinct zones: (I) initial heating and pressing, (II) additive removal, (III) heating up to the sintering temperature, and (IV) final sintering, as illustrated in Fig. 2. Considering the effect of dwell time, it became evident that longer durations resulted in more significant compaction of the powder mixture. Additionally, although the heating rate and time for all samples are approximately similar, the displacement curve of the paraffin-containing sample increased dramatically in the first zone. Such observation indicates that the consolidation of sample 10P at lower temperatures follows an intensified trend, compared to sample 10St. This can be attributed to the fact that paraffin evaporates at a temperature range of approximately 50 to 70 °C, leading to more noticeable changes in displacement. However, during the final stage, the densification behavior in the last sintering step appears to be similar for both 10St and 10P samples. Therefore, the lower water adsorption in 10P can be attributed to its higher green density before the final sintering step.

Fig. 3 illustrates the XRD results of the as-SPSed samples, indicating that their X-ray diffraction patterns are nearly identical. Considering the evaporation of paraffin at the beginning of the sintering process, there is a lower intensity of the carbon peak compared to samples containing starch. However, with increased sintering time in the starch-containing samples, carbon had more time to evaporate, resulting in sharper peaks of the magnesium phase. In other words, with the increase in sintering time in starch-containing samples, the intensity of the Mg phase peak decreases. Moreover, it is evident that in comparing the obtained patterns from different samples, differences in the quantities of Mg and MgO phases are evident.

Despite the high temperatures applied during the sintering process and the combustion of carbon additives, the XRD patterns show evidence of carbon-based residues remaining after the combustion of starch.

Fig. 4 depicts the FESEM images of the polished and etched cross-sections of the as-sintered samples. The micrographs show that the samples containing starch have a more homogeneous microstructure than the paraffin-containing sample. Thread-like phases within the

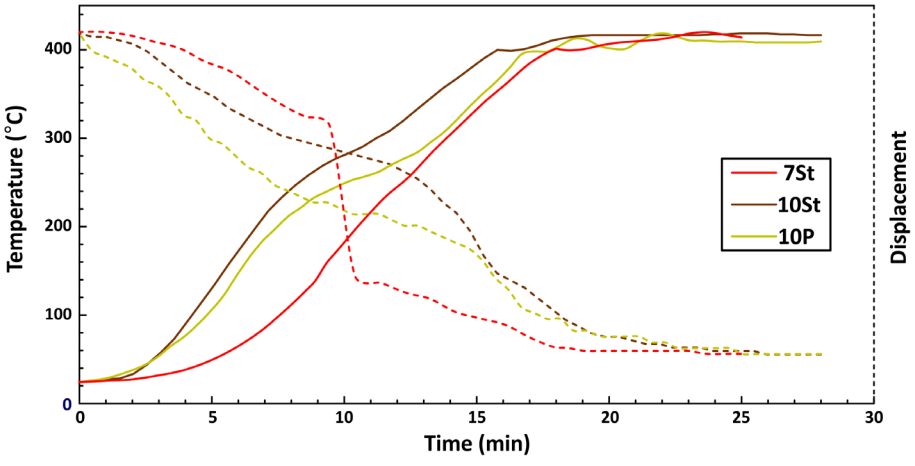


**Fig. 2.** Displacement-time-temperature (DTT) diagrams of the sintered samples.

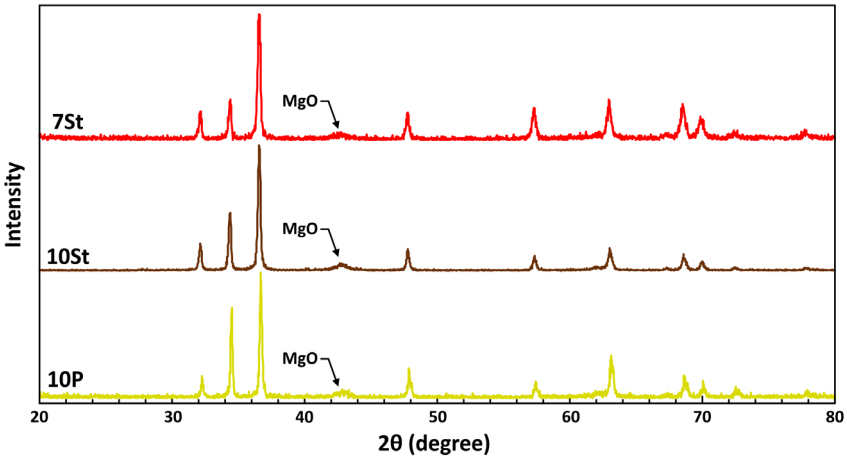


**Fig. 3.** XRD patterns of the sintered samples.

magnesium matrix can be attributed to inter-particle boundaries. According to data from the back-scattered electron (BSE) detector as well as the related EDS elemental maps, these regions exhibit a notable concentration of oxides, mainly secondary magnesium oxide characterized by white spherical structures and carbon.

When comparing the presence of porosity, the starch-containing sample sintered for 7 min exhibits slightly higher porosity than the one sintered for 10 min. This phenomenon may be attributed to insufficient time for porosity removal through atomic diffusion. Additionally, it is observed that porosities remain in the paraffin-containing sample even after 10 min of sintering, indicating that longer dwell times are needed for this type of additive.

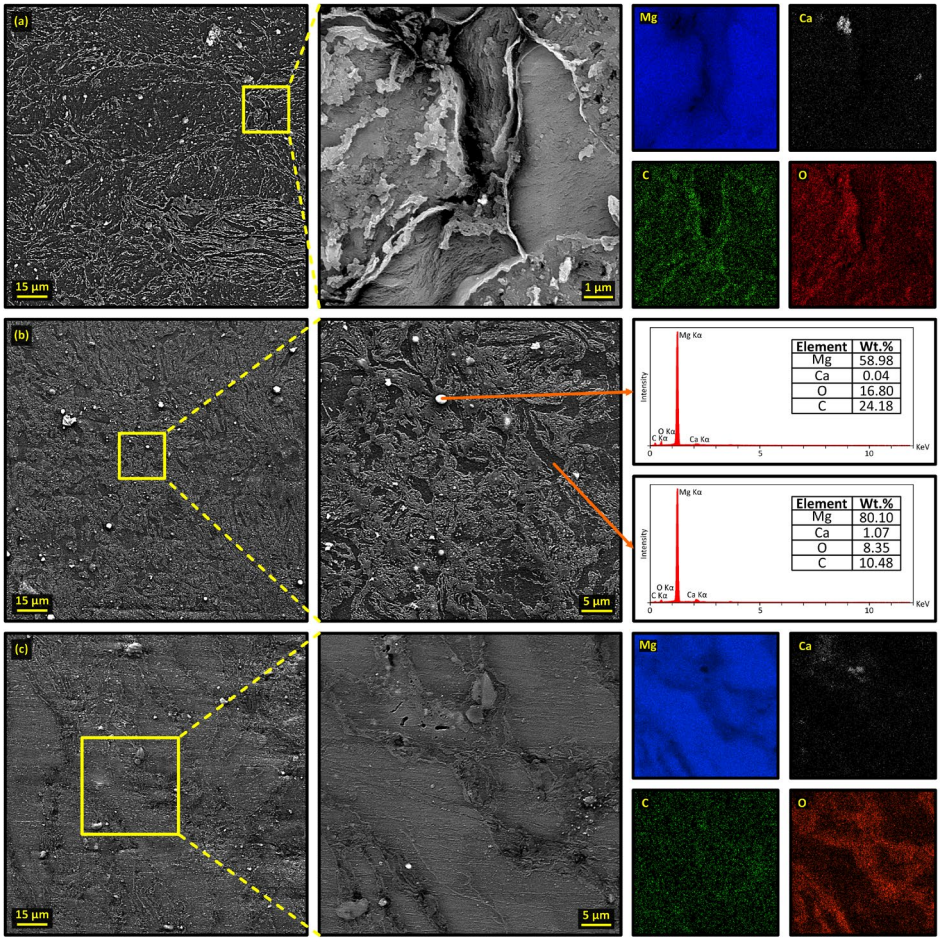


**Fig. 4.** FESEM micrographs of the SPSed samples: a) 7St, b) 10St, and c) 10P.

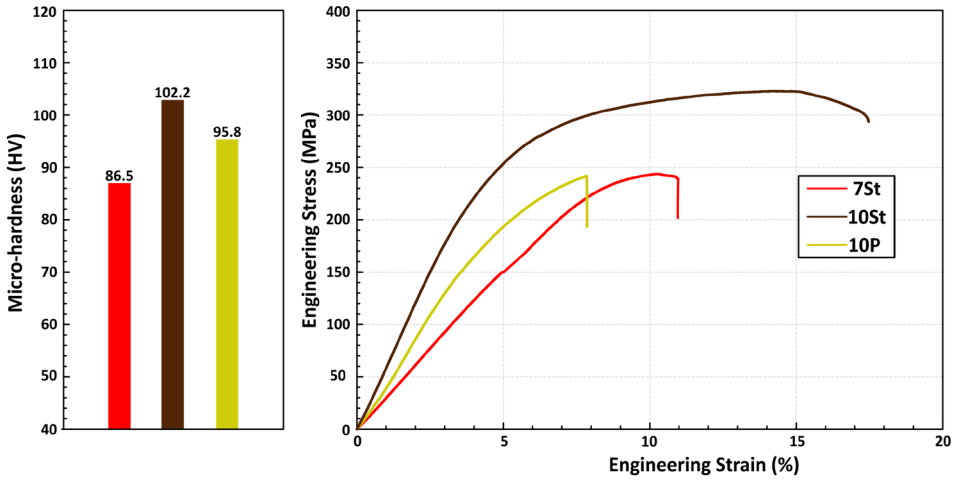


**Fig. 5.** The engineering stress-strain curves and measured micro-hardness of the sintered samples.

The stress-strain curves and the micro-hardness results of the SPSed samples are illustrated in Fig. 5. It is evident that as the sintering time increases from 7 to 10 minutes in starch-containing samples, a significant increase in micro-hardness is observed. This phenomenon can be attributed to a lower level of porosity within the structure of the sample 10St. In addition, the micro-hardness value of sample 10St is higher than that of the paraffin-containing sample (10P). This difference in micro-hardness is attributed to a higher concentration of magnesium oxide within the structure of 10St, which results from the presence of oxygen-containing compounds in the starch.

Notably, the stress-strain curve for sample 7St displays irregular behavior, which can be ascribed to the poor mechanical properties of the alloy. It is important to acknowledge that porosity and structural flaws directly exert an influence on mechanical properties. Additionally, an abundance of carbon (additive residues) can make the structure brittle, reducing mechanical properties such as elongation and strength.

In the comparative analysis of the samples that were sintered for 10 min with different additives, it is imperative to consider the nature and characteristics of these additives. Specifically, paraffin evaporates at relatively lower temperatures and thoroughly exits the sintering chamber. In contrast, starch burns and leaves an ash-like residue. This residue not only departs from the material's structure but also expands, potentially thwarting the compaction during the compression test. Based on the stress-strain diagrams and the mechanical properties results shown in Table 3, it is observed that the compressive strength of the samples increases with prolonged sintering time.

**Table 3.** Mechanical properties of the as-SPSed samples.

| Sample code | Elongation (%) | Yield stress (MPa) | Compressive strength (MPa) |
|---|---|---|---|
| 7St | 3.2 | 125 | 192.5 |
| 10St | 11.2 | 220 | 322.5 |
| 10P | 2.2 | 190 | 241.7 |

It can be concluded that magnesium oxide contributes to the strengthening and precipitation hardening of starch-containing samples, whereas in paraffin-containing samples, the primary mechanism enhancing mechanical properties is believed to be densification and porosity removal.

## 4. Conclusions

In this research, the effects of dwell time and additive type on mechanically alloyed Mg-Ca powders consolidated through spark plasma sintering were examined. The main conclusions are summarized as follows:

- Increasing the dwell time from 7 to 10 min results in improved hardness, elongation, and overall mechanical properties of the as-SPSed sample.
- In the case of a dwell time of 10 minutes, starch demonstrates superior performance compared to paraffin, exhibiting better mechanical properties and a finer microstructure.
- In starch-containing samples, magnesium oxide plays a key role as a strengthening and precipitation-hardening factor during the sintering process. In contrast, in paraffin-containing samples, the mechanism mainly involves densification and porosity removal.

## CRediT authorship contribution statement

**Parisa Golmohammadi:** Writing – original draft, Software, Formal Analysis, Validation, Investigation.
**Ahmad Bahmani:** Writing – review & editing.
**Nader Parvin:** Supervision, Funding acquisition, Writing – review & editing, Project administration.
**Behzad Nayebi:** Writing – original draft, Writing – review & editing, Visualization, Methodology, Conceptualization, Investigation.

## Data availability

The data underlying this article will be shared on reasonable request to the corresponding author.

## Declaration of competing interest

The authors declare no competing interests.

## Funding and acknowledgment

The authors would like to thank the ArtaMag research core and Arta Magnesium Parsian Engineering Co. for their help and support during the study. We would also like to express our sincere gratitude to Mr. Kabiri from the Materials and Energy Research Center (MERC, Karaj, Iran) for his invaluable guidance and support.

## References

[1] N. Sharma, G. Singh, P. Sharma, A. Singla, Development of Mg-Alloy by Powder Metallurgy Method and Its Characterization, Powder Metall. Met. Ceram. 58 (2019) 163–169. https://doi.org/10.1007/s11106-019-00060-5.

[2] J. Song, J. She, D. Chen, F. Pan, Latest research advances on magnesium and magnesium alloys worldwide, J. Magnes. Alloy. 8 (2020) 1–41. https://doi.org/10.1016/j.jma.2020.02.003.

[3] Y. Yang, X. Xiong, J. Chen, X. Peng, D. Chen, F. Pan, Research advances in magnesium and magnesium alloys worldwide in 2020, J. Magnes. Alloy. 9 (2021) 705–747. https://doi.org/10.1016/j.jma.2021.04.001.

[4] J. Song, J. Chen, X. Xiong, X. Peng, D. Chen, F. Pan, Research advances of magnesium and magnesium alloys worldwide in 2021, J. Magnes. Alloy. 10 (2022) 863–898. https://doi.org/10.1016/j.jma.2022.04.001.

[5] J. Tan, S. Ramakrishna, Applications of magnesium and its alloys: A review, Appl. Sci. 11 (2021) 6861. https://doi.org/10.3390/app11156861.

[6] S.V.S. Prasad, S.B. Prasad, K. Verma, R.K. Mishra, V. Kumar, S. Singh, The role and significance of Magnesium in modern day research-A review, J. Magnes. Alloy. 10 (2022) 1–61. https://doi.org/10.1016/j.jma.2021.05.012.

[7] J. Bai, Y. Yang, C. Wen, J. Chen, G. Zhou, et al., Applications of magnesium alloys for aerospace: A review, J. Magnes. Alloy. 11 (2023) 3609–3619. https://doi.org/10.1016/j.jma.2023.09.015.

[8] A. Maqbool, N.Z. Khan, A.N. Siddiquee, Towards Mg based light materials of future: properties, applications, problems, and their mitigation, J. Manuf. Sci. Eng. 144 (2022) 030801. https://doi.org/10.1115/1.4051678.

[9] M. Ahmadi, S.A.A.B. Tabary, D. Rahmatabadi, M.S. Ebrahimi, K. Abrinia, R. Hashemi, Review of selective laser melting of magnesium alloys: advantages, microstructure and mechanical characterizations, defects, challenges, and applications, J. Mater. Res. Technol. 19 (2022) 1537–1562. https://doi.org/10.1016/j.jmrt.2022.05.102.

[10] A. Bahmani, M. Lotfpour, M. Taghizadeh, W.-J. Kim, Corrosion behavior of severely plastically deformed Mg and Mg alloys, J. Magnes. Alloy. 10 (2022) 2607–2648. https://doi.org/10.1016/j.jma.2022.09.007.

[11] R. Chalisgaonkar, Insight in applications, manufacturing and corrosion behaviour of magnesium and its alloys – A review, Mater. Today Proc. 26 (2020) 1060–1071. https://doi.org/10.1016/j.matpr.2020.02.211.

[12] S.K. Esamael, A.A. Fatalla, Analysis of Effect of Alloying Magnesium by Powder Metallurgy on Mechanical Properties : Review, J. Adv. Med. Dent. Sci. Res. 9 (2021) 100–106.

[13] E. Ghasali, M. Alizadeh, M. Niazmand, T. Ebadzadeh, Fabrication of magnesium-boron carbide metal matrix composite by powder metallurgy route: Comparison between microwave and spark plasma sintering, J. Alloys Compd. 697 (2017) 200–207. https://doi.org/10.1016/j.jallcom.2016.12.146.

[14] J.A.M. Carvalho, G. Domingues, M.T. Fernandes, N. Larcher, A.A. Ribeiro, J.A. Castro, Evaluation of MgZnCa Alloys Fabricated Via Powder Metallurgy for Manufacturing Biodegradable Surgical Implants, JOM. 73 (2021) 2403–2412. https://doi.org/10.1007/s11837-021-04739-2.

[15] M. Behera, D.B. Panemangalore, R. Shabadi, Additively Manufactured Magnesium-Based Bio-Implants and their Challenges, Trans. Indian Natl. Acad. Eng. 6 (2021) 917–932. https://doi.org/10.1007/s41403-021-00241-y.

[16] L. Yang, T. Wang, C. Liu, Y. Ma, L. Wu, et al., Microstructures and mechanical properties of AZ31 magnesium alloys fabricated via vacuum hot-press sintering, J. Alloys Compd. 404–406 (2021) 8. https://doi.org/10.1016/j.jallcom.2005.05.002.

[17] S. Gonzaga, A. Molina, R. Guardián, H. Martínez, E.V. Vélez, J.S.O. Tapia, Synthesis of Magnesium-Based Alloys by Mechanical Alloying for Implant Applications, Coatings. 13 (2023) 1–15. https://doi.org/10.3390/coatings13020260.

[18] P. Golmohammadi, F. Saljooghi, A. Bahmani, N. Parvin, B. Nayebi, On the synthesis and sintering behavior of a novel Mg-Ca alloy, Part I: Mechanical alloying, Synth. Sinter. 2 (2022) 131–137. https://doi.org/10.53063/synsint.2022.23118.

[19] M. Tokita, Progress of spark plasma sintering (SPS) method, systems, ceramics applications and industrialization, Ceramics. 4 (2021) 160–198. https://doi.org/10.3390/ceramics4020014.

[20] M. Sakkaki, M. Naderi, M. Vajdi, F. Sadegh Moghanlou, A. Tarlani Beris, A simulative approach to obtain higher temperatures during spark plasma sintering of ZrB2 ceramics by geometry optimization, Synth. Sinter. 3 (2023) 248–258. https://doi.org/10.53063/synsint.2023.34178.

[21] X.Y. Li, Z.H. Zhang, X.W. Cheng, G.J. Huo, S.Z. Zhang, Q. Song, The development and application of spark plasma sintering technique in advanced metal structure materials: A review, Powder Metall. Met. Ceram. 60 (2021) 410–438. https://doi.org/10.1007/s11106-021-00254-w.

[22] N. Sezer, Z. Evis, S.M. Kayhan, A. Tahmasebifar, M. Koç, Review of magnesium-based biomaterials and their applications, J. Magnes. Alloy. 6 (2018) 23–43. https://doi.org/10.1016/j.jma.2018.02.003.

[23] R. Liu, W. Wang, H. Chen, Z. Lu, W. Zhao, T. Zhang, Densification of pure magnesium by spark plasma sintering-discussion of sintering mechanism, Adv. Powder Technol. 30 (2019) 2649–2658. https://doi.org/10.1016/j.apt.2019.08.012.

[24] M. Saravana Kumar, S. Rashia Begum, M. Vasumathi, C.C. Nguyen, Q. Van Le, Influence of molybdenum content on the microstructure of spark plasma sintered titanium alloys, Synth. Sinter. 1 (2021) 41–47. https://doi.org/10.53063/synsint.2021.1114.

[25] Z.-Y. Hu, Z.-H. Zhang, X.-W. Cheng, F.-C. Wang, Y.-F. Zhang, S.-L. Li, A review of multi-physical fields induced phenomena and effects in spark plasma sintering: Fundamentals and applications, Mater. Des. 191 (2020) 108662. https://doi.org/10.1016/j.matdes.2020.108662.

[26] H.G. Mohammed, T.M.B. Albarody, M. Mustapha, N.M. Sultan, H.K.M. Al-Jothery, Investigate the effect of process parameters of magnetic inductively assisted spark plasma sintering (SPS) of iron oxide (Fe3O4) on microstructure behaviour – Part I, Mater. Today Proc. 42 (2021) 2106–2112. https://doi.org/10.1016/j.matpr.2020.12.293.

[27] A.S. Mukasyan, A.S. Rogachev, D.O. Moskovskikh, Z.S. Yermekova, Reactive spark plasma sintering of exothermic systems: A critical review, Ceram. Int. 48 (2022) 2988–2998. https://doi.org/10.1016/j.ceramint.2021.10.207.

[28] M. Suarez, A. Fernandez, J.L. Menendez, R. Torrecillas, H.U. Kessel, et al., Challenges and Opportunities for Spark Plasma Sintering: A Key Technology for a New Generation of Materials', Sintering Applications, Intech. (2013). https://doi.org/10.5772/53706.